

observed in testing. Stresses in the soil around the pipe are relatively low, but fail above and below the pipe as gravity is applied. In general, the pipe performance is excellent when pressures and loads are within the design limits as currently applied by Ameron (modified from the 2009 proposed limitations) and robust as pressures and loads exceed the design limits.

## 7. REFERENCES

1. ANSI/AWWA C304-07, AWWA Standard for Design of Prestressed-Concrete Cylinder Pipe.
2. Simulia, Abaqus Analysis User's Manual, Abaqus 6.11.
3. T.J. McGrath, "95240 – Richland Chambers Pipeline – Analysis of Bends, Soil Properties" 19 January 1996.
4. Mueller, R., Dana, W.R., and Hall, S. (2009) "Introducing PressureCast™ Steel Pipe – A New Combination of Proven Materials and Designs", Proceedings of ASCE Conference, Pipelines 2009
5. AWWA (2004). AWWA Manual of Water Supply Practices – Manual M11 Steel Pipe – A Guide for Design and Installation, 4th ed., American Water Works Association, Denver, CO.

## Dynamic Behavior of Buried Flexible Pipes of Varying Thickness Using the Shaking Table Test

Kawabata, T.<sup>1</sup>, Sonoda, Y.<sup>2</sup>, Mohri, Y.<sup>3</sup>, Ariyoshi, M.<sup>4</sup>, and Iwasaki, Y.<sup>5</sup>

<sup>1</sup> M.ASCE, Ph.D., Professor, Graduate School of Agricultural Science, Kobe University, 1-1, Rokkodai, Nada, Kobe, 657-8501, JAPAN; PH +81-78-803-5902; kawabata@kobe-u.ac.jp

<sup>2</sup> Graduate Student, Graduate School of Agricultural Science, Kobe University; yysonoda@gmail.com

<sup>3</sup> M.ASCE, Ph.D., National Institute for Rural Engineering, Kannondai 2-1-2, Tsukuba, Ibaragi, 305-8609, JAPAN; PH +81-29-838-7574; ymohri@affrc.go.jp

<sup>4</sup> Researcher, National Institute for Rural Engineering; ariyoshi@affrc.go.jp

<sup>5</sup> Graduate Student, Graduate School of Agricultural Science, Kobe University; zen\_vo\_ov@yahoo.co.jp

### ABSTRACT

In designing a pipeline, deflection and stress of the pipe are calculated through structural analysis based on bending ring stiffness  $EI/D^3$ . The pipes with equivalent bending ring stiffness would have the same behavior in design. However, it is easily understandable that the behavior of pipe may be influenced not only by  $EI/D^3$ , but also by the relationships between  $E$  and  $I$ .

In this paper, shaking table test for buried flexible pipes were conducted to evaluate the effects of pipe thickness on the dynamic behavior. Some pipes having approximately equivalent bending ring stiffness and different thickness were used. In this experiment, these pipes were buried in the laminar box and shaken by horizontal sine wave.

As a result, it was found that the larger bending strain and radial stress of the pipe occurred with the thinner wall. This result suggests that the probability of the buckling of the pipe is higher on thinner pipes. It is evident that the pipelines for irrigation should be designed in consideration of this fact.

### INTRODUCTION

Main irrigation pipeline networks extend over 4,500 km in Japan. 14 % of those networks in length require immediate repair works. The behavior of a buried pipeline or any underground structure is significantly influenced by the surrounding ground, the construction method employed, and various properties of the backfill material used. Particularly, an increased application of flexible pipes having a low stiffness is expected in the near future because of their good workability and economy reason. Such flexible pipes having a low stiffness with thin wall tend to be easily deformed

and buckling may occur as a result of an external force applied as overburden pressure.

The pioneering principles of mechanics on the flexible pipe were reported to verify and determine its horizontal and vertical deflections, bending moments, and tangential thrusts by Marston (1930) and Spangler (1941). Full-scale experiments on flexible culverts were conducted and the design formula developed from the load hypothesis was verified by Spangler. The hypothesis assumed the passive horizontal pressures to show parabolic distribution on the sides of a pipe. In Japan, Marston-Spangler theory is applied to the design standard of the pipeline by the Ministry of Agriculture, Forestry and Fisheries (2010).

In the current Japanese design standard for the irrigation pipeline, deflection and stress of the pipe are calculated through structural analysis (closed-form analysis) based on bending ring stiffness  $EI/D^3$  ( $E$ : elastic modulus,  $I$ : geometrical moment of inertia,  $D$ : diameter of pipe). The pipes with equivalent bending ring stiffness would have the same behavior in design. However, Kawabata et al. (2010) conducted vertical loading tests using some flexible pipes having equivalent bending ring stiffness and found that the probability of buckling of the pipe may be higher on thinner pipes.

In this paper, shaking table test for buried flexible pipes were conducted to evaluate the effects of pipe thickness on the dynamic behavior. The steel pipe of thickness 1.92 mm, the PVC pipe of thickness 7.23 mm and the high density polyethylene pipe (HDPE pipe) of 11.52 mm were used. These pipes had approximately equivalent bending ring stiffness. In this experiment, these pipes were buried in the laminar box and shaken by 2 Hz horizontal sine wave.

## EXPERIMENTAL PROGRAM

**Model pipe.** The properties of pipes are shown in Table 1. The steel pipe of thickness 1.92 mm, the PVC pipe of thickness 7.23 mm and the high density polyethylene pipe (HDPE pipe) of 11.52 mm were used. These pipes had approximately equivalent bending ring stiffness and diameter.

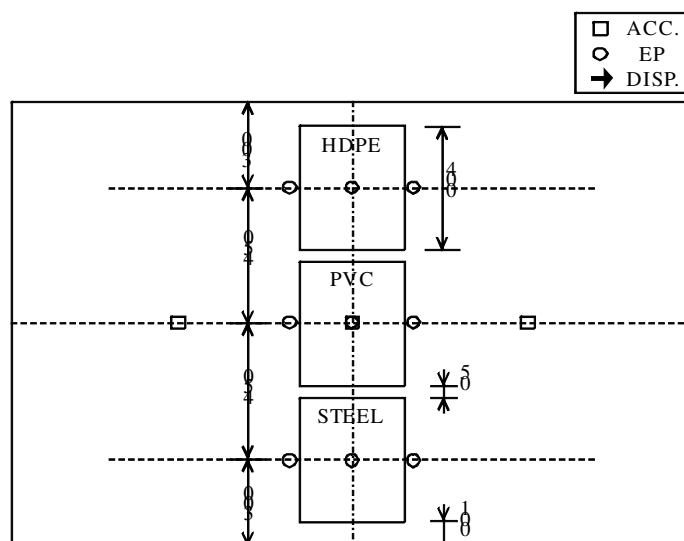
**Experimental setup.** Figure 1 shows the experimental setup. The laminar box (1990 × 1500 × 970 mm) containing model ground and model pipes were installed on the shaking table. The pipes were backfilled with silica sand in the relative density of 30 %. The grain size distribution of silica sand is shown in Figure 2. In order to evaluate the deformation of the pipe accurately, 64 strain gauges were attached circumferentially to the inner and outer surface of each pipe at interval of 11.25 degrees. In addition, the displacement transducers were installed in the four directions. The configuration of them is shown in Figure 3.

**Experimental cases.** Table 2 shows the experimental cases. In Stage-1, three different pipes (Case-1~3) were backfilled together. In Stage-2, three pipes (Case-4~6) were set on the concrete foundation and backfilled together. Schematic diagram of concrete foundation is shown in Figure 4.

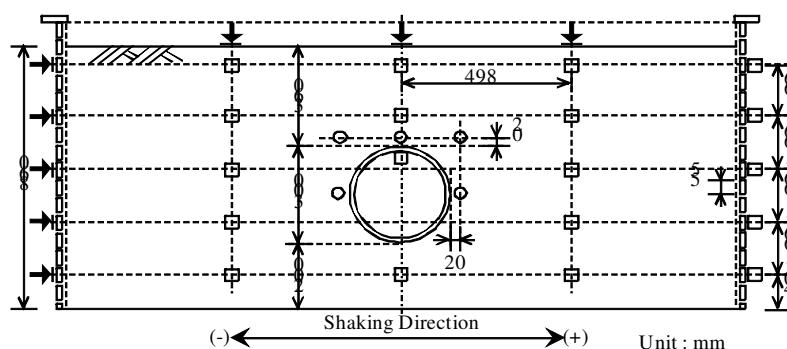
**Experimental procedure.** In this experiment, 2 Hz horizontal sine wave applied to the shaking table. Figure 5 shows input wave. The shaking was applied at 600gal and the shaking duration was about 20 seconds.

**Table 1. Properties of pipes**

	Thickness $t$ (mm)	Diameter $D$ (mm)	Thickness/Dia. (%)	Elastic modulus $E$ (N/mm <sup>2</sup> )	Bending ring stiffness $EI/D^3$ (N/mm <sup>2</sup> )
STEEL	1.92	301.9	0.6	164399	0.00358
PVC	7.23	309.2	2.3	3155	0.00334
HDPE	11.52	311.8	3.7	1007	0.00392



(a) Ground plane



(b) Cross section

**Figure 1. Experimental Setup**

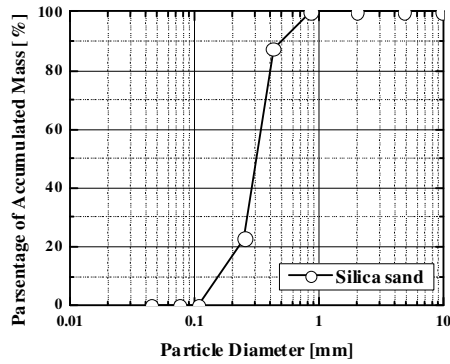


Figure 2. Grain size distribution of silica sand

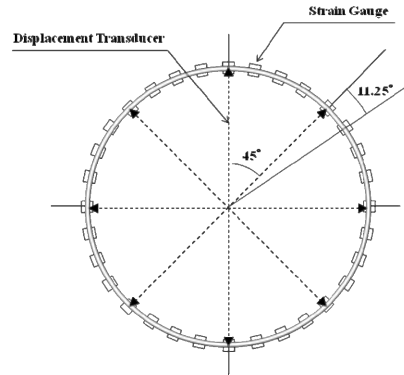


Figure 3. Configuration of strain gauges and displacement transducers

Table 2. Experimental cases

	Case	Material	Foundation
Stage-1	Case-1	STEEL	Blank
	Case-2	PVC	
	Case-3	HDPE	
Stage-2	Case-4	STEEL	Concrete
	Case-5	PVC	
	Case-6	HDPE	

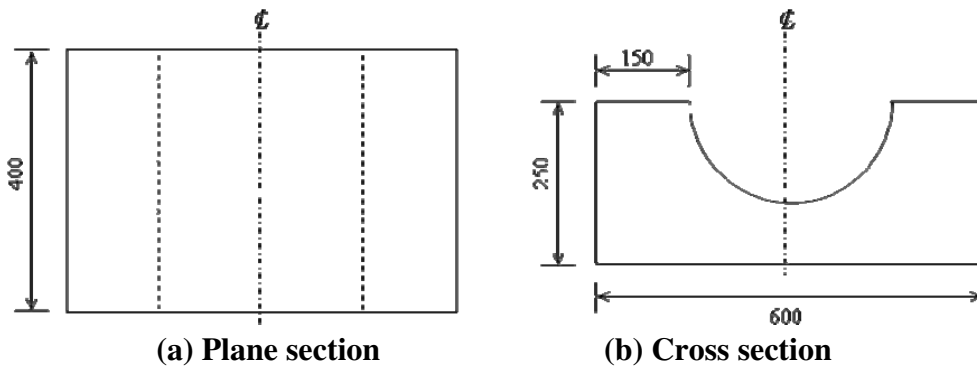


Figure 4. Schematic diagram of concrete foundation

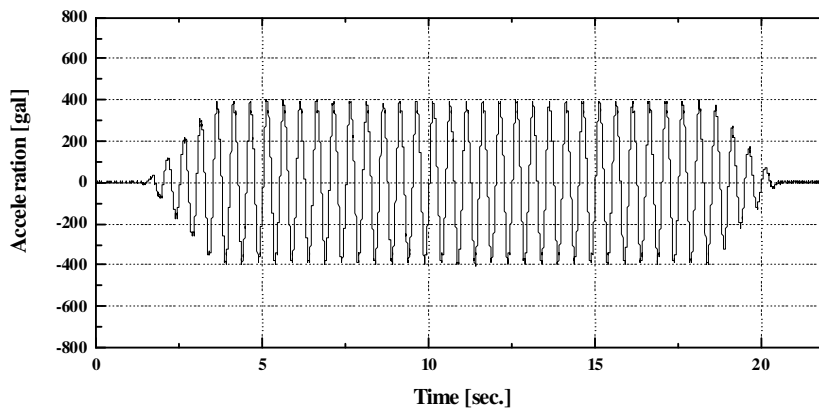


Figure 5. Input wave

## EXPERIMENTAL RESULTS

**Pipe deflection.** Figure 6 shows the responses of pipe deflection during shaking. The vertical deflection when the pipe deforms vertically is shown by the positive value.

In Case-1~3, the vertical deflection decreased and the horizontal deflection increased gradually. That is, the pipes deformed horizontally. This behavior was given by the negative dilation of the loose ground. The responses of the pipe deflection in the direction of 45 degrees and 135 degrees were large in the beginning of the shaking. In Case-1, the maximum horizontal deflection was 3.08 mm. On the other hand, the maximum deflection in the direction of 45 degrees was 6.31 mm. This result means that the vibration of the ground has a heavier affect on the pipe deformation in the oblique direction than in the vertical and horizontal direction. The 45 degrees deflection in Case-3 containing the thickest pipe (HDPE pipe) was the smallest in these cases. It is likely that the response of pipe deformation is dependent on the pipe thickness.

In Case-4~6, the vertical deflection showed positive value and the horizontal deflection showed negative value. That is, the pipes deformed vertically. It is considered that the concrete foundation prevents the pipes from deforming horizontally. The 45 degrees and 135 degrees deflection in Case-4~6 were significantly smaller than in Case-1~3.

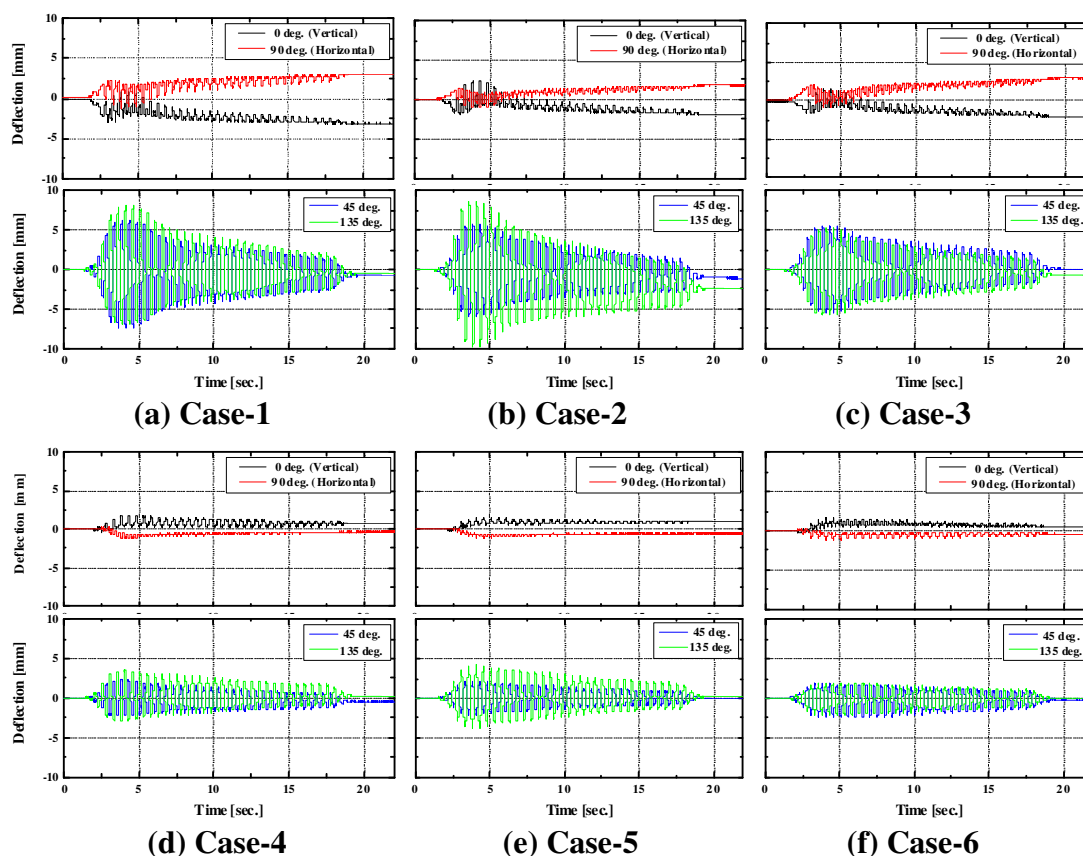


Figure 6. The response of pipe deflection

**Bending strain.** Figure 7 shows the response acceleration of pipe and response of bending strains at the position of 45 degrees and 90 degrees of pipes. Bending strain is calculated by dividing the difference between inner circumferential strain and outer circumferential strain. The scale of vertical axis was adjusted with the thickness of pipes.

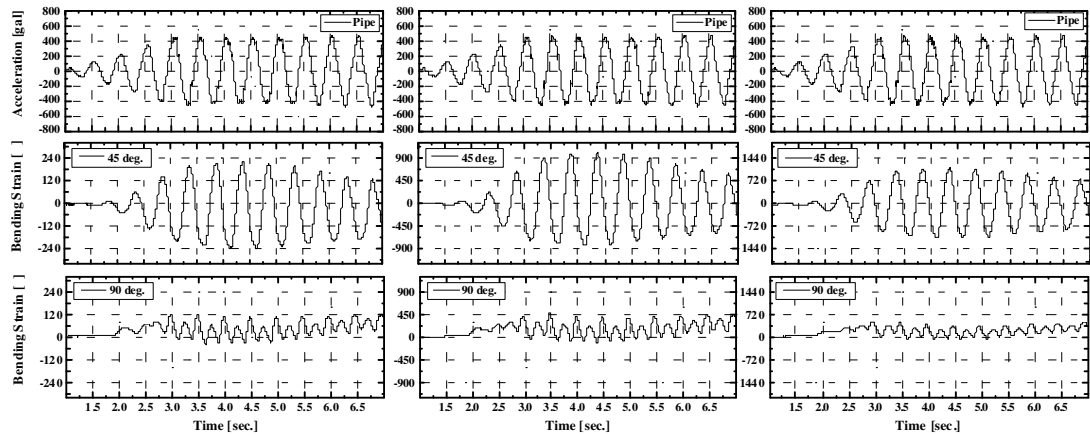
In Case-1~3, the bending strains at 45 degrees reached the maximum values when the acceleration of pipe reached the minimum values. In other words, the positive bending strains were generated at 45 degrees when the pipe was shook to the left side. This behavior was given by the shear deformation of the surrounding ground. On the other hand, the positive bending strains were generated at 90 degrees when the acceleration of pipe reached the maximum values and minimum values. The values of the strains were significantly smaller than at 45 degrees. Judging from these results, it is considered that the shaking of the pipe has heavier affect on the bending stress at the 45 degrees than at 90 degrees. The bending strain at 45 degrees in Case-3 containing HDPE pipe was the smallest in these cases.

In Case-4~6, the bending strains at 45 degrees showed the same pattern as in Case-1~3. However, the strains at 90 degrees in Case-4~6 became much larger than in Case-1~3. The negative bending strains were generated at 90 degrees when the acceleration of pipe reached minimum values. It is likely that the stress concentration was acted at the spring line of pipe by the concrete foundation. The bending strain at 90 degrees in Case-6 containing HDPE pipe was by far the smallest in these cases.

Figure 8 shows the bending strain distribution at the 3.11 seconds from beginning of the shaking. At this times, the accelerations of pipes in all cases reached nearly maximum value. The results in Case-1~3 indicate together on Figure 8 (a) and those in Case-4~6 indicate on Figure 8 (b). The scale of the strain was adjusted with the thickness of the pipes based on PVC pipe.

The shapes of the bending strain distributions were almost similar in Case-1~3. The negative bending strains were distributed around the position of 45 degrees and 225 degrees of pipes. The positive bending strains were distributed around 135 degrees and 315 degrees. These distributions were given by the elliptical deformation of pipe in the oblique direction. It is likely that buried pipes subjected to earthquake vibration mainly deform in the direction of 45 degrees or 135 degrees. The values of the strains in Case-1 containing STEEL pipe were the largest and in Case-3 containing HDPE pipe were the smallest in these cases. Judging from these results, it is considered that yielding fracture is more likely to occur at these positions of thinner pipes.

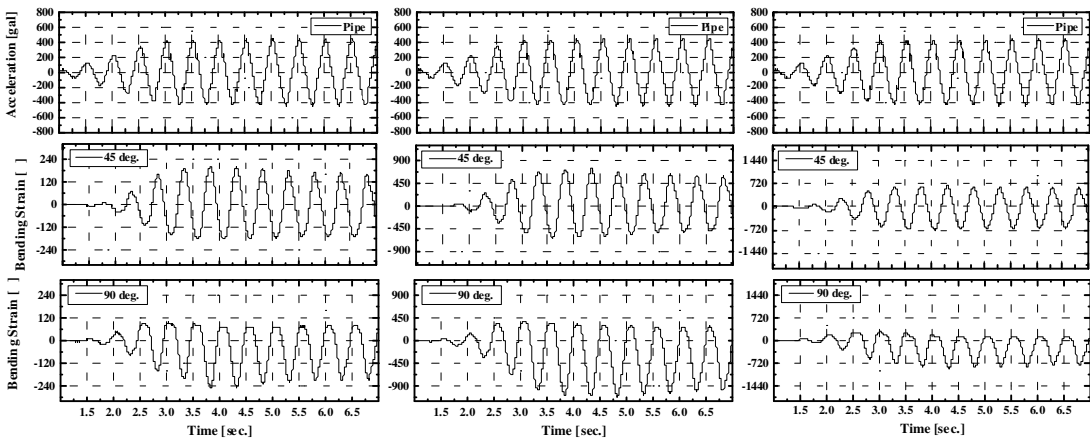
In Case-4~6, the shapes of the bending strain distributions at the upper half of the pipe were almost similar to that in Case-1~3. At the lower half of the pipes, the negative strains were distributed around the position of 270 degrees and positive strains were generated at the area between 90 degrees and 135 degrees. It is likely that the stress concentration was acted at the 270 degrees by the edge concrete foundation when the ground sheared to the left. Little bending strains were distributed around the bottom of the pipe. This result was be given by the concrete foundation restraint. The values of the strains in Case-4 containing STEEL pipe were the largest and in Case-6 containing HDPE pipe were the smallest in these cases. These trends were the same as in Case-1~3.



(a) Case-1

(b) Case-2

(c) Case-3

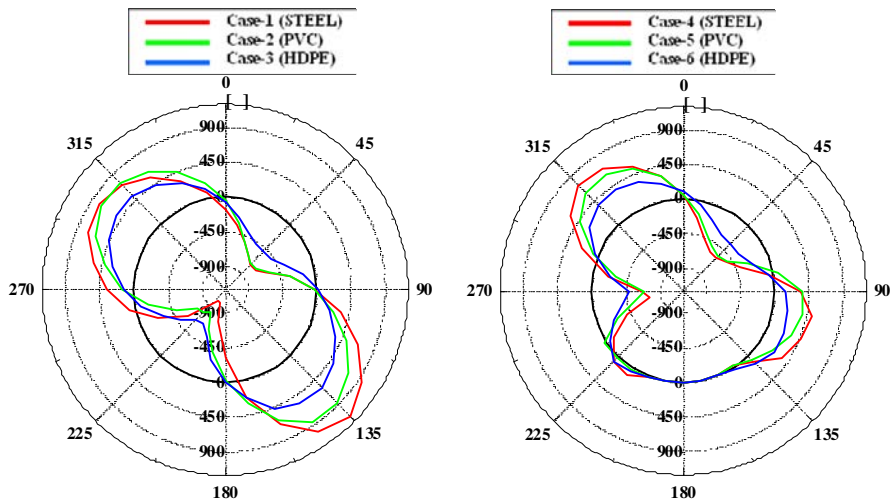


(d) Case-4

(e) Case-5

(f) Case-6

Figure 7. Response acceleration and response of bending strains



(a) Case-1~3

(b) Case-4~6

Figure 8. The bending strain distribution at the 3.11 second

**Radial stress.** Figure 9 shows the response acceleration of pipe and response of radial stresses at the position of 45 degrees and 90 degrees. The value of the radial stress is positive for the tensile force. Radial stress is computed by multiplying the radial strain by the elastic modulus. Radial stress is expressed by the average value between inner circumferential strain and outer circumferential strain. It represents the circumferential strain at the center of the wall thickness, or strain at neutral axis in elastic theory.

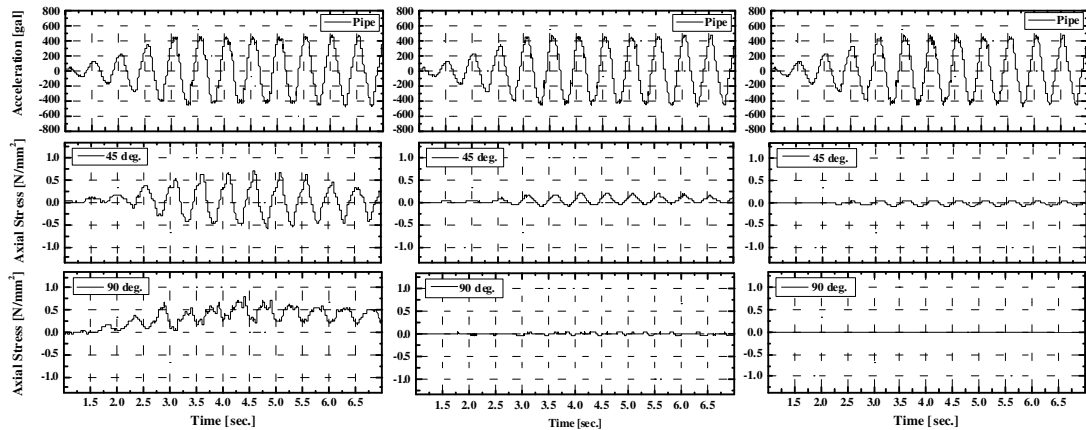
In Case-1~3, the radial stresses at 45 degrees reached the maximum values when the acceleration of pipe reached the maximum values. In other words, the tensile radial stresses were generated at 45 degrees when the pipe was shook to the left side. This behavior was given by the shear deformation of the surrounding ground. The tensile radial stresses were generated at 90 degrees when the acceleration of pipe reached the minimum values. The variations of the radial stresses at 90 degrees were smaller than at 45 degrees. These results mean that the shaking of the pipe affects heavier the radial stress at the 45 degrees than at 90 degrees. The radial stress in Case-1 containing STEEL pipe was the largest and in Case-3 containing HDPE pipe was the smallest in these cases. Judging from these results, it is considered that radial stress become larger on thinner pipe during the shaking.

In Case-4~6, the radial stresses at 45 degrees showed the same pattern as in Case-1~3. However, the radial stresses at 90 degrees in Case-4~6 became much larger than in Case-1~3. Large tensile stress in Case-4 containing STEEL pipe was generated at 90 degrees. It is likely that tensile radial stress is generated by the stress concentration.

Figure 10 shows the radial stress distribution at the 3.11 seconds from beginning of the shaking. At this times, the accelerations of pipes in all cases reached nearly maximum value. The results in Case-1~3 indicate together on Figure 10 (a) and those in Case-4~6 indicate on Figure 10 (b).

In Case-1~3, the tensile radial stresses were distributed around the position of 45 degrees and 225 degrees of pipes. The compressive stresses were distributed around 135 degrees. The shapes of these distributions were opposite to those of the bending strain distributions. It is likely that the tensile radial stress is generated where the negative bending strain is generated. The value of radial stress was large. That is, the radial stresses were larger on thinner pipe. Large radial stresses were non-uniformly distributed in Case-4 containing STEEL pipe. Judging from these results, it is considered that buckling may occur on the thin pipe compared to thick pipe during the shaking.

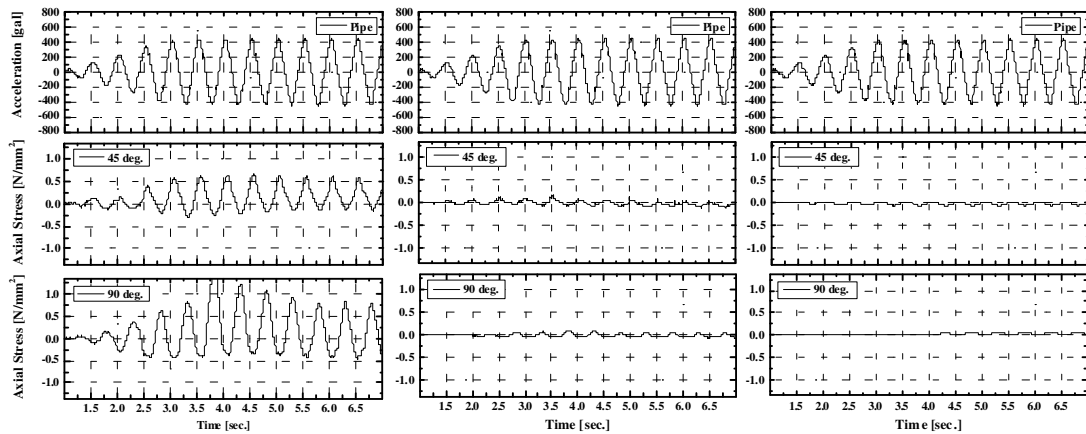
In Case-4~6, the tensile radial stresses were distributed around the position of 45 degrees and 270 degrees of pipes. It is likely that the stress concentration was acted at the 270 degrees by the edge concrete foundation when the ground sheared to the left. Little radial stresses were distributed around the bottom of the pipe. This result was given by the concrete foundation restraint. The values of the radial stresses in Case-4 containing STEEL pipe were the largest in these cases and they were non-uniformly distributed. These trends were the same as in Case-1~3.



(a) Case-1

(b) Case-2

(c) Case-3

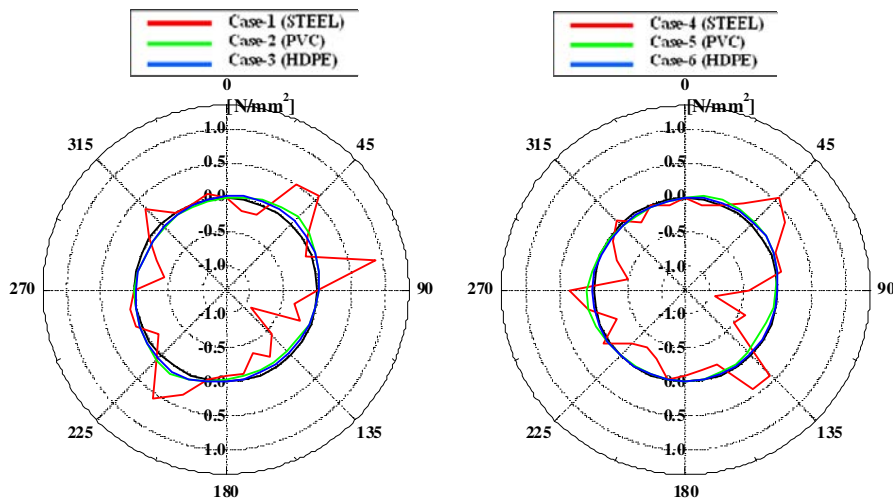


(d) Case-4

(e) Case-5

(f) Case-6

Figure 9. Response acceleration and response of radial stresses



(a) Case-1~3

(b) Case-4~6

Figure 10. The radial stress distribution at the 3.11 second